Chemical Physics 520 (2019) 88–99

Contents lists available at ScienceDirect

Chemical Physics

journal homepage: www.elsevier.com/locate/chemphys

A four-dimensional Numerov approach and its application to the vibrational eigenstates of linear triatomic molecules – The interplay between anharmonicity and inter-mode coupling

Ulrich Kuenzer, Thomas S. Hofer*

Theoretical Chemistry Division, Institute of General, Inorganic and Theoretical Chemistry, Center for Chemistry and Biomedicine, University of Innsbruck, Innrain 80-82, A-6020 Innsbruck, Austria

A B S T R A C T

An adapted formulation of the grid-based Numerov approach to solve Schrödinger's equation has been extended to four-dimensional systems and applied to problems in vibrational spectroscopy. The advantage of this novel implementation is that no approximations or assumptions with respect to the wavefunctions are required and the achieved accuracy at a given stencil size is only limited by the selected grid-spacing. To validate this approach the vibrational eigenstates and the corresponding wavenumbers of the linear molecules CO_2, BeH_2 and HCN were investigated. Based on a potential energy grid at CCSD(T)/cc-pVnZ (n = T, Q) level all fundamental wavenumbers could be reproduced with deviations of less than 1% of the experimental values. Furthermore, the hierarchical application of a one- to four-dimensional Numerov treatment provides detailed information about the increasing influence of inter-mode coupling in addition to the inherent account for anharmonic contributions. The associated vibrational states are eigenfunctions of the Numerov matrix eigenvalue problem. Since no vibrational basis functions have to be applied in this approach, the respective eigenstates are characterized using isosurfaces of the wavefunctions in the hyperplane $x_4 = 0$. This enables the direct examination of the individual wavefunctions via suitable visualization tools and the assignment of the respective vibrational quantum numbers.

1. Introduction

Theoretical approaches to vibrational spectroscopy are an increasingly active field of research correlated with the development of the computational infrastructure in the last decades. The most basic method for the prediction of vibrational properties is the harmonic frequency approximation and variations thereof [1–3]. These approaches are known to mostly overestimate the frequencies due to the neglection of anharmonicity and inter-mode coupling. Since these effects are of crucial importance to obtain accurate results a variety of different approaches was proposed, covering a broad field of applications. A widely used method is Vibrational Perturbation Theory (VPT2) [4–6], in which the potential close to the minimum is approximated using a polynomial representation of higher order. This ansatz leads to improved results compared to the harmonic approximation, but it has been shown that it is not able to fully represent potentials displaying a strong degree of anharmonicity [7,8]. A different approach is the Vibrational Self Consisting Field (VSCF) ansatz [9–12]. It uses, analogous to the Hartree-Fock SCF, an ansatz in which the coupling between the modes is strongly approximated. Various corrections of this approach, like PT-VSCF (Perturbation Theory-VSCF)[13,14], CC-VSCF (Coupled Cluster-VSCF)[15] or CI-VSCF (Configuration Interaction-VSCF) [16] were proposed. These improved methods yield a higher accuracy but at the same time the computational demand is dramatically increased, leading to limitations in the treatable system size. For this reason a number of approaches based on VSCF with focus on a computational efficient procedure for the investigation of larger chemical systems have been developed [17–22].

VSCF- and VPT2-like methods are based on potential energy grids and respective derivative data, that are subsequently interpolated to obtain a continuous representation of the underlying potential energy surface. In addition, there exist also grid-based approaches evaluating the wavefunctions only on the provided data-points. These methods have been shown to lead to reliable results [23–26], while at the same time having only small computational demand. The field of application of these methods is not limited to vibrational spectroscopy but includes also the description of the electronic density in atoms and small molecules [27–34]. The difference between these grid based methods is the way to approximate the Hamiltonian, leading to variations in the resulting matrix eigenvalue equation. Using comparatively simple algebraic methods all eigenstates can be calculated at once from diagonalisation of the matrix. In general this methods are only limited by the matrix size and the resulting computational time for the eigenvalues and eigenvectors. The larger the provided potential energy grids, the more memory and computational time is needed.

One widely used grid-based method is the Numerov approach

* Corresponding author.
E-mail address: T.Hofer@uibk.ac.at (T.S. Hofer).

https://doi.org/10.1016/j.chemphys.2019.01.007
Received 13 November 2018; Received in revised form 21 December 2018; Accepted 6 January 2019
Available online 09 January 2019
0301-0104/

[35–40]. Here the second derivative is approximated using finite differences on an equispaced grid [41]. Recently, an improved Numerov approach was proposed [42], being able to chose the accuracy of the method, while at the same time the computational effort was reduced by using a sparse matrix formulation. Another commonly used method is the discrete variable representation (DVR) [43–45,25,26], where the grid and the corresponding matrix are created applying a chosen basis. Depending on the selected basis sets, the resulting gridpoints differ [46,47]. For the most common basis sets the Laplace operator leads to partly dense matrices [48,46]. Especially for higher dimensions this may lead to a large amount of data. For this purpose a variety of approaches were developed cropping the respective basis, enabling to solve up to six-dimensional vibrational problems[49–51]. For such high dimensional vibrational applications the used basis sets have to be adapted to the investigated chemical system. The Colbert Miller DVR (CM-DVR) [25], which corresponds to an infinite-order finite-difference approximation is similar to the improved Numerov method [42] but with a higher computational demand due to the partly dense matrix. The CM-DVR is known to lead to accurate estimations of energies and eigenvalues already on small grids [37], but up to now is only formulated for three dimensions. The Numerov and DVR approaches are strongly connected to the so called Finite Basis Representation (FBR) approaches [44,52–54], being a member of the spectral method family.

A third related method to solve the Schrödinger equation is the Chebyshev collocation approach [23,24]. In this method the grid points are placed at the roots of the Chebyshev polynomials and are therefore not equally spaced. Nevertheless, it was stated that the accuracy of the method is slightly better than that of the standard Numerov method [37]. Due to the increased accuracy of the improved Numerov method [42] it can be expected that it leads to more accurate results. The (improved) Numerov method was shown to predict the experimentally determined vibrational frequencies of H_2 and H_2O within $\leqslant 1\%$ using correlated *ab initio* based potential energy information [42]. The Numerov scheme applied to DFT calculations on hybrid level lead to accurate results in predicting the IR frequencies (fundamental and first overtone) of the OH-vibrational modes of methanol and phenol [55] as well. The underlying potential energy grids were created using single point energy calculations along the respective vibrational normal modes.

The normal mode vectors used for the scan directions are computed via the harmonic approximation in a previous calculation. Although the calculation of the potential energy grid is perfectly parallelisable it is still the bottleneck of the Numerov analysis, especially in higher dimensions. The Numerov method (as well as the other grid-based methods) have been formulated for problems in one, two and three dimensions [37,38,56]. This paper focuses on the four-dimensional Numerov scheme and its application to triatomic linear systems. To assess the accuracy of this approach the method is benchmarked against a four-dimensional harmonic oscillator system as well as against experimental and previous theoretical results for CO_2, BeH_2 and HCN. Furthermore, the resulting wavefunctions are used to assign the quantum numbers to the respective vibrational frequencies, which is outlined in the results section.

2. Methods

2.1. Adapted Numerov method

The Numerov Method [35,36] was introduced in the 1920s and represents a numerical framework to solve ordinary differential equations of the form

$$\Delta\psi(x) = f(x)\psi(x), \tag{1}$$

on an equidistant grid, with Δ corresponding to the Laplace operator. By choosing the function f such as

$$f(\mathbf{x})\psi(\mathbf{x}) = \frac{2m}{\hbar^2}(E - V(\mathbf{x}))\psi(\mathbf{x}), \tag{2}$$

the Numerov framework can be applied to the time independent Schrödinger equation with V describing the potential, m the effective mass and E the energy eigenvalue. In [37,38,56] the Numerov method was reformulated as a matrix eigenvalue problem and extended to two and three dimensions. The key advantages of this framework are, that:

(i) no approximations/assumptions on the form of the wave-function Ψ_N have to be introduced,
(ii) no choice/definition of basis functions $\{\phi\}$ is necessary, and,
(iii) a consequence of the latter, no matrix elements of the form $\langle\phi_i|\hat{O}|\phi_j\rangle$ arise from the combination of basis functions ϕ_i, ϕ_j, ... with an operator $\hat{O}$.

However, in its original form the Numerov approaches suffer the same problem as the widely employed Colbert-Miller discrete variable representation (CM-DVR) approach [25,26], which by definition requires a partly dense-filled matrix associated with a comparably high computational demand and large memory requirements. Especially for problems in higher dimensions or subject to large potential energy grids this quickly leads to a serious limitation of the treatable system size.

In [42] an adapted Numerov approach was proposed, dramatically reducing the memory demand and the execution time. This method is shortly summarized in this paper and extended to a four-dimensional formulation. A more detailed description for one, two and three dimensions can be found in [42]. The presented approach considers all vibrational modes, whereas the coupling of vibrational and rotational degrees of freedom is presently not considered.

To apply the algorithm to vibrational problems in higher dimensions it is necessary that the grid spacing is equal along all degrees of freedom. To guarantee an equidistant grid of normal mode combinations with different reduced masses, mass-weighted coordinates are used. The reduced mass of a normal mode $Q_i \in \mathbb{R}^{3K}$, where K denotes the number of atoms of the chemical system can be calculated by

$$\mu_i = \sqrt{\sum_{j=1}^{3K} Q_{i,j}^2 \cdot m_{(\lfloor (j-1)/3 \rfloor)+1}}, \tag{3}$$

with $\lfloor ... \rfloor$ corresponding to the floor function. In general, the reduced mass μ_i is different for the individual normal modes. For this reason mass-weighted coordinates are introduced as $x_i^{mw} = \sqrt{\mu_i} x_i$. In the following, unless not mentioned explicitly x_i refers to mass-weighted coordinates.

The accuracy of the results depends primarily on the accuracy of the underlying potential energy surface (PES), typically calculated applying GGA-DFT or higher levels of theory. The PES is created applying mass weighted coordinates along the respective normal modes of the chemical system. Since each calculation of the potential energy scan is just a single point energy calculation at a given configuration, this step is perfectly parallelisable.

In addition, the order of the stencil applied in the Numerov method is the second factor determining the accuracy of the resulting eigenvalues and eigenvectors basing on the PES. The associated potential energy matrix $\mathbb{V}$ is a diagonal matrix with the respective potential energy for each configuration being an entry along the diagonal. The employed size of the grid and the applied levels of theory for the different chemical systems are addressed in Section 2.3.

2.1.1. One dimension

As mentioned the Numerov method is a grid-based method employing K equispaced points x^i, $i = 1, ..., K$, following the short notation $\psi(x^i) = \psi_i$ and $\psi(x^{i\pm k\cdot h}) = \psi_{i\pm k}$, with k being a natural number. All ψ_i with $i < 1$ and $i > K$ are considered zero, applying Dirichlet (zero) boundary conditions. In one dimension the Laplace operator Δ

simplifies to $\partial^2/\partial x^2$.

Summing up the two Taylor series for $x + h$ and $x - h$ and substituting $\partial^2/\partial x^2 \psi(x) = f(x)\psi(x)$ leads to the expression

$$\psi_{i+1} - 2\psi_i + \psi_{i-1} = h^2 f^i \psi^i + 2\sum_{k=2}^{N} \frac{h^{2k}}{(2k)!}\psi_i^{(2k)} + \mathcal{O}(h^{2N+2}). \tag{4}$$

In Eq. (4) the desired accuracy N can be chosen. In the next step, all occurring derivatives are approximated using finite difference expressions [41]. As an example the resulting equation for $N = 3$ is shown:

$$f_i\psi_i = \frac{1}{h^2}\left(\frac{1}{90}\psi_{i+3} - \frac{3}{20}\psi_{i+2} + \frac{3}{2}\psi_{i+1} - \frac{49}{18}\psi_i + \frac{3}{2}\psi_{i-1} - \frac{3}{20}\psi_{i-2} + \frac{1}{90}\psi_{i-3}\right) + \mathcal{O}(h^6). \tag{5}$$

The number of neighboring points considered determine the stencil size and thus, the accuracy of the approximation of the second derivative. Considering ψ_i as entries of a vector $\boldsymbol{\psi}$, the equations for all $\boldsymbol{\psi}_i$ can be combined to a matrix equation

$$\mathbb{f}\boldsymbol{\psi} = \mathbb{A}\boldsymbol{\psi}, \tag{6}$$

with $\mathbb{A}$ being a matrix filled with the respective coefficients near the diagonal and $\mathbb{f}$ being a diagonal matrix. Next, Eq. (6) is applied to the Schrödinger equation according to Eq. (2) which leads to the eigenvalue equation in matrix form given as

$$(\mathbb{A} + \mathbb{V})\boldsymbol{\psi} = \mathbb{H}\boldsymbol{\psi} = E\boldsymbol{\psi}, \tag{7}$$

with the diagonal potential matrix $\mathbb{V}$ and the sparse filled and symmetric Hamiltonian matrix $\mathbb{H}$. In this approach the eigenvalues are guaranteed to be real, while the eigenvectors are orthogonal to each other. Furthermore, the matrix inversion, being a mandatory step in the original formulation of the matrix Numerov procedure [35–37] can be avoided. Comparing the performance of the adapted version against the original formulation highlighted, that effectively the same results are obtained while a substantial reduction of the computational effort could be achieved [42]. The key feature of the Numerov approach that no approximation or assumption with respect to the actual form of the wavefunction has to be made (*i.e.* no choice of basis function, no product approach for problems in higher dimensions, etc.) is retained. Thus, in case of higher dimensional problems a full account of vibrational correlation effects is ensured, which corresponds to an accurate treatment of inter-mode coupling in addition to an inherent consideration of anharmonic contributions on a quantum mechanical level.

It should be noted, that the size of the Hamiltonian matrix soley depends on the number of grid-points. Thus, the application of larger stencils only changes the number of non-zero entries in the matrix, but not the overall size of the eigenvalue problem. The smallest possible stencil for the approximation of the second derivative considers only one neighboring point in the direction $\pm h$. It was demonstrated that this level of accuracy is inferior compared to the corresponding Chebyshev collocation method and the CM-DVR implementations [37]. However, extending the stencil to include more neighboring points leads to a substantial improvement of the achievable accuracy [55,42].

Fig. 1 illustrates the relation between a one-, two- and three-dimensional Numerov treatment at the example of CO_2. The treament of just a single mode enables the investigation of anharmonic effects on the respective vibrational mode (Fig. 1a; red: bending; blue: sym. stretch; green: asym. stretch). By considering two vibrations in a 2d-Numerov implementation coupling contributions between the considered modes are taken into account in addition to the treatment of anharmonicity. Fig. 1b shows an exemplary 2d-potential energy surface along with the resulting wave functions of the ground state ψ_{00} and the two first excited states ψ_{10} and ψ_{01}.

Further increase of the dimensionality enables a hierarchical consideration of inter-mode coupling contribuitons. In the 3d-case both the potential and the wave functions can only be depicted in form of isosurfaces as shown in Fig. 1c for three vibrational modes of CO_2. The 4d-case on the other hand is too complex to enable a depiction of the potential and wave functions without loss of information.

2.1.2. Four-dimensional approach

The derivation of the four-dimensional Numerov approach starts with the formula

$$\begin{aligned}\Delta\psi(x_1, x_2, x_3, x_4) &= \left(\frac{\partial^2}{\partial(x_1)^2} + \frac{\partial^2}{\partial(x_2)^2} + \frac{\partial^2}{\partial(x_3)^2} + \frac{\partial^2}{\partial(x_4)^2}\right)\psi(x_1. x_2, x_3, x_4) \\ &= f(x_1, x_2, x_3, x_4)\psi(x_1, x_2, x_3, x_4).\end{aligned} \tag{8}$$

As the Numerov method is a numerical method to solve the Schrödinger equation, the problem is being solved on a grid $x_1^i,\ x_2^j,\ x_3^k,\ x_4^l$ with the index starting at 0 and K_{x1}, K_{x2}, K_{x3}, K_{x4} describing the respective number of grid points in each direction. To keep the following derivation as simple as possible a short notation is introduced: $\psi(x_1^i, x_2^j, x_3^k, x_4^l) = \psi_{i,j,k,l}$ and $\psi(x_1^{i\pm m\cdot h}, x_2^{j\pm n\cdot h}, x_3^{k\pm o\cdot h}, x_4^{l\pm p\cdot h})$.

$$= \psi_{i\pm m,\, j\pm n,\, k\pm o,\, l\pm p}$$

Analogous to the lower dimensional case the derivation of the Numerov method starts with a sum of Taylor series, namely the 16 Taylor series of $\psi_{i\pm1,\, j\pm1,\, k\pm1,\, l\pm1}$ in all combinations. Rearrangement and application of the identity in (8) then yields

$$\begin{aligned}\sum_{m,n,o,p\in\{-1,1\}} \psi_{i+m,j+n,k+o,l+p} - 16\psi_{i,j,k,l} &= 8h^2 f_{i,j,k,l}\psi_{i,j,k,l} \\ &+ 16\sum_{s=2}^{N} \frac{h^{2s}}{(2s)!} \\ &\sum_{\alpha+\beta+\gamma+\delta=s} \frac{(2s)!}{(2\alpha)!(2\beta)!(2\gamma)!(2\delta)!} \\ &\frac{\partial\psi_{i,j,k,l}^{(2s)}}{\partial x_1^{(2\alpha)}\partial x_2^{(2\beta)}\partial x_3^{(2\gamma)}\partial x_4^{(2\delta)}} + \mathcal{O}(h^{2N+2}),\end{aligned} \tag{9}$$

with N being the desired accuracy. After the accuracy N is chosen, the derivatives on the right side of the truncated Eq. (9) have to be approximated using finite differences [41]. The respective derivatives are then approximated using stencils applied to the particular gridpoints, *e.g.* the second derivative of the function f in x_0 is approximated by $f''(x_0) = (f(x_1) - 2f(x_0) + f(x_{-1}))/h^2 + \mathcal{O}(h^2)$. The approximation of the single terms in the truncated Eq. (9) has to be in line with the general accuracy of $\mathcal{O}(h^{2N+2})$ (or $\mathcal{O}(h^{2N})$ after dividing the truncated equation by h^2). Consider a desired accuracy of $2N + 2$, then the approximation of the terms being multiplied with h^{2s} has to be of order $t = N - s + 1$ to guarantee the desired accuracy. Furthermore, the mixed derivatives have to be approximated combining the respective one-dimensional stencils [41]: The higher the desired accuracy, the bigger is the stencil to be used. Consider a stencil size of $2o + 1$. The index of the four-dimensional stencil C is then indexed from $-o$ to o in all four dimensions. Given are the one-dimensional stencils for the approximation of the derivative in every direction, named S^{x_1}, S^{x_2}, S^{x_3} and S^{x_4}. Then the entries of the four-dimensional stencil are calculated as

$$C_{i,j,k,l} = S_i^{x_1}\cdot S_j^{x_2}\cdot S_k^{x_3}\cdot S_l^{x_4} \text{ for } i,\ j,\ k,\ l \in [-o, o] \subset \mathbb{N} \tag{10}$$

If in one direction no derivative has to be considered, the stencil S is assumed as $S_i = 0$ for $i \neq 0$ and $S_0 = 1$. The symmetry of the Taylor series and the stencils for even derivatives can be further used to reduce the effort in constructing the stencil. After all derivatives have been expressed via the associated stencils, the respective sum yields the associated matrix $\mathbb{A}$. Although in one dimension a three-point stencil exists, in higher dimensions only five-point and higher stencils lead to suitable results.

In order to conserve the eigenvalue character of the Numerov approach, the four-dimensional grid has to be represented in vector form. This yields $\psi_{i,j,k,l} = \psi_{i\cdot K_{x2}\cdot K_{x3}\cdot K_{x4} + j\cdot K_{x3}\cdot K_{x4} + k\cdot K_{x4} + l}$, assuming the indices starting with zero and K_{x_i} representing the number of grid points in the

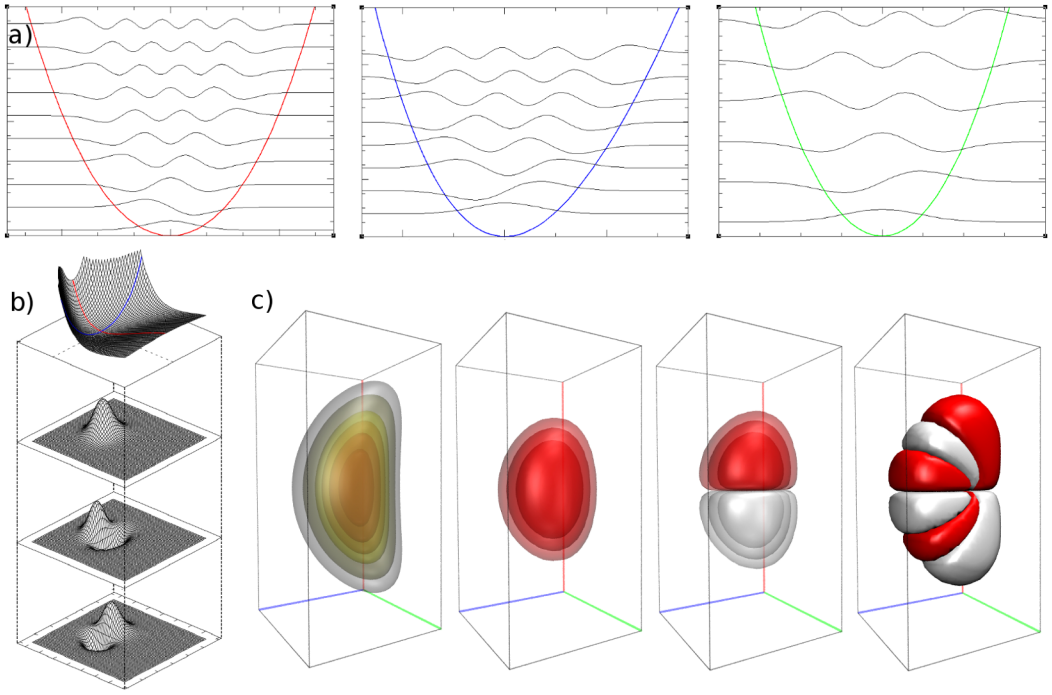

Fig. 1. Schematic visualisation of the Numerov procedure in (a) one-, (b) two- and (c) three dimensions. The potentials of the normal modes of CO_2 (red: bending, blue: sym. stretch, green: asym. stretch) and the corresponding wavefunctions are shown (2D: ψ_{00}, ψ_{10}, ψ_{01}, 3D: ψ_{000}, ψ_{100}, ψ_{120}). The isosurfaces of the wavefunctions in three dimensions are drawn at $\pm$ 0.1, $\pm$0.01 and $\pm$ 0.001. The isosurfaces of the potential are representing 5, 10, 15, 20, 30, 40 kcal/mol, respectively. The visualization of the four-dimensional case is not possible without loss of information.

respective direction. Next, the finite differences and the potential have to be on the same side of the equation to yield the matrix to be solved as an eigenvalue problem. In one dimension the resulting matrix $\mathbb{A}$ is filled only near the diagonal. Due to transformation of the four-dimensional grid to a one-dimensional vector, the resulting matrix in four dimensions is always a block matrix in which the particular blocks have a similar structure than the whole matrix in the three-dimensional case. At the same time only the blocks near the diagonal are filled, analogous to the non-zero entries in the one-dimensional case.

With higher dimensions the eigenvalue problem becomes more difficult to solve. The number of non-zero entries (using the same stencil size) increases with each dimension. The large amount of data in higher dimensions can lead to numerical instabilities as well as large memory requirements. To prevent the latter specialized algorithms have to be applied.

2.2. Algorithms

A large variety of algorithms are available to find the solutions of a matrix eigenvalue problem. Due to the sparse matrix formulation of the 4d-Numerov approach an algorithm supporting sparse matrices is highly desirable. As the matrix size increases exponentially with every dimension an iterative solver, *e.g.* Lanczos based algorithms, are to be preferred. The Numerov method in lower dimensions was implemented using the Intel MKL [57] library as well as the Armadillo ARPACK library [58,59]. In the four-dimensional case the Intel MKL Library was not able to solve the eigenvalue problem due to its size. Therefore, the ARPACK routine had to be applied. However, since also the ARPACK routine was close to its capacity limit, the executed calculations (presented in Section 3) were only possible using an 5-point stencil per dimension, whereas a 7-point stencil proved already too demanding.

2.3. Test systems

In this section the investigated chemical systems are presented. First, a benchmarking of the 4d Numerov approach has been carried out by comparing the energy eigenvalues obtained for a 4d harmonic oscillator with the associated analytical solutions. Next, the method was applied to the target systems CO_2, BeH_2 and HCN, which are among the most common examples for linear triatomic molecules. In all cases the Numerov procedure was applied in a hierarchical fashion, starting with a one-dimensional treatment accounting for anharmonicity but entirely disregarding inter-mode coupling. Next, each mode was coupled to the other normal modes by successively increasing the number of coupled modes, leading to a set of 2d-, 3d- and 4d-Numerov analyses. The results have been compared to the wavenumbers obtained from the harmonic approximation and where available to VPT2 results as well as to other literature sources. The individual variation in the respective wave-numbers upon increasing the number of coupled normal modes have been analyzed in detail. All quantum chemical calculations were executed using Gaussian(09) [60], figures were created using VMD [61].

2.3.1. CO_2

The carbon dioxide molecule was chosen because it is one of the most studied molecules with four different vibrational modes. Due to its linear structure it has 4 vibrational normal modes. Therefore, it is an ideal system to test the four-dimensional approach of the Numerov method. The system was investigated applying a $49 \times 49 \times 25 \times 25$ grid. Due to symmetry considerations (point group $D_{\infty h}$) not all grid points had to be calculated. Four different accuracy levels have been considered, namely:

- B3LYP/6-311++G(3df,3pd) [62,63]
- MP2/6-311++G(3df,3pd) [64,3,63]
- MP2/cc-pVTZ [64,3,65]
- CCSD(T)/cc-pVTZ [66,3,65].

For each theory level/basis set the molecular structure was optimized and the normal modes were calculated in the following. For all

calculations a grid spacing of 0.02 Å was assumed. Applying mass-weighted coordinates leads to step sizes adapted by the respective reduced mass in all dimensions. In addition to a comparison to the harmonic approximation the Numerov results have also been compared to results obtained at VPT2 level of theory in case of MP2 and B3LYP.

2.3.2. BeH_2

As second example beryllium hydride was chosen. It was investigated to highlight similarities and differences with respect to CO_2 and due to the availability of IR data in the literature. All calculations were performed on CCSD(T)/cc-pVQZ level [66,3,65] on a $49 \times 49 \times 21 \times 17$ grid. In this case a grid spacing of 0.04 Å was assumed prior to the application of mass-weighting.

2.3.3. HCN

The third example consists of three different atoms. HCN was chosen to assess the performance of the Numerov-approach in a different symmetry group ($C_{\infty v}$) than the first two examples. Additionally, the C-N triple bond increases the difficulty to accurately compute the potential energy surface of this system. All calculations were executed on CCSD(T)/cc-pVTZ [66,3,65] level using a $45 \times 45 \times 47 \times 15$ grid. The grid spacing was also assumed as 0.04 Å prior to transforming the grid to mass-weighted coordinates.

2.4. Mode assignment

The Numerov approach calculates the eigen-energies and the respective wavefunctions directly from the potential energy grid without the need to define any basis functions. Although the eigenstates are typically ordered according to the increasing eigenvalues, the actual four-dimensional quantum numbers required for the mode assignment remain unknown.

In one dimension it is straightforward to assign a certain frequency to the respective excited state. The number of nodes of the wavefunction is equivalent to the excitation of the respective state. In two dimensions this classification shows first challenges: Considering the state (1 1) of a harmonic oscillator, shown in Fig. 2 it is clear that a simple count of nodal planes along the axes $x_1 = 0$ or $x_2 = 0$ does not lead to the correct result, whereas in most other cases (*e.g.* state (2 0)) this approach is successful. Because of this fact it is necessary to visually inspect the wavefunctions to determine the respective excitation. This was done in the examples of CO_2, BeH_2 and HCN. For both CO_2 and BeH_2 the wavenumber of the first excitation of the asymmetric stretch mode is known to be over 2100 cm^{-1}, while in case of HCN the C–H stretching mode is above 3000 cm^{-1}. All states below 2100 (or 3000 for HCN) wavenumbers can thus be projected onto the hyperplane $x_4 = 0$ without loss of information. In this hyperplane the wavefunctions can be visualized applying isosurfaces in three-dimensional space, for instance using the program VMD [61]. This isosurfaces are in the following used to assign the respective quantum numbers to the different states. The majority of states can be easily assigned, while in some cases the assignment proved ambiguous. In higher dimensions the principal axes defined by the different normal modes are not always parallel to the directions of the resulting nodal surfaces, which makes an automated recognition of quantum numbers highly challenging.

3. Results

In this section the results of the performed calculations are presented. As mentioned in the section above for all target systems and theory levels a one-, two-, three-, and four-dimensional Numerov analysis was carried out. Thus, with increasing dimension the influence of mode-mode coupling can be analyzed in a step-wise procedure. The resulting wavefunctions were then used to assign the obtained wavenumbers to the respective excited states, which are compared to results given in the literature.

3.1. 4d-Harmonic oscillator

To investigate the convergence properties of the Numerov implementation, the eigenvalues of a 4d-harmonic oscillator have been calculated and compared to the analytical results. The respective force constants in the different dimensions were $k_{x1} = 700$, $k_{x2} = 800$, $k_{x3} = 900$ and $k_{x4} = 1000 \frac{kcal}{molA^{\circ 2}}$. The latter is a typically value corresponding to an O–H bond, while the other force constants represents weaker interactions (*e.g.* C–H or N–H bonds). To investigate the effective order of the applied five-point stencil grids with 11^4, 15^4, 19^4, 23^4, 27^4, 31^4 and 35^4 points have been considered in the interval $[-0.5A^{\circ}, 0.5A^{\circ}]^4$. The 35^4 point grid leads to total number of 1500625 gridpoints and a matrix size of 1500625^2 corresponding to $2.25 \cdot 10^{12}$ matrix elements. Due to the sparse character of the Numerov approach only 79849401 entries of the matrix are non-vanishing, corresponding to $\approx 0.0035\%$. The deviations from the analytical results observed for different grid-sizes are listed in Table 1 for the first, the fifth and the tenth eigenvalue.

In case of the largest grid with $h = 0.0294$ Å the deviation in the first and fifth eigenvalue (*i.e.* the ground and fourth excited state) from the analytical value are 0.00097 and 0.00171 kcal/mol (*i.e.* 0.3 and 0.6cm^{-1}), *i.e.* well below one wavenumber. In case of the CO_2 molecule an even smaller grid spacing of $h = 0.02$ Å was applied (prior to mass-weighting), in case of BeH_2 and HCN the spacing was 0.04 Å, which too is well within the acceptable margin.

It is also important to note that the practical order ($n \approx 3$) is lower than the theoretical order ($\mathcal{O}(h^4)$), which indicates that the eigenvalue solver is an additional limiting factor. This is mainly due to the fact that in addition to the eigenvalues also the eigenvectors have been computed. In case knowledge of the eigenvalues is sufficient, a number of more efficient algorithms are available.

3.2. CO_2 – Carbon dioxide

The CO_2 molecule was calculated at three different theory levels, being B3LYP, MP2 and CCSD(T) (two different basis sets were used in the MP2 case). The resulting frequencies of the vibrational modes obtained from a 4d-Numerov treatment are summarized in Table 2 and compared to results obtained via the harmonic approximation and VPT2 data. The Numerov calculations were executed using a 5-point stencil. It can be seen that the deviations to experimental data are reduced with increasing level of theory. At CCSD(T)-level all deviations from the experimental values are $\leqslant 1\%$.

Also the results at MP2 and DFT level show good agreement with

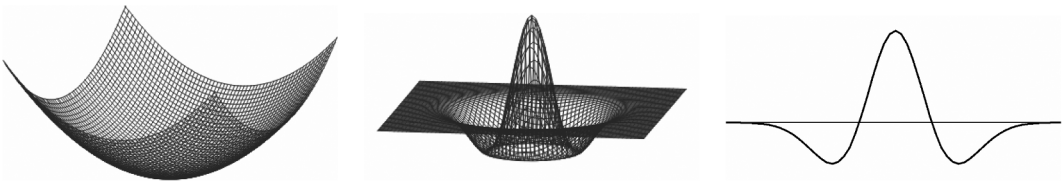

Fig. 2. Potential energy surface of a 2d-harmonic oscillator (left), the corresponding wavefunction of the (1 1) state (middle) and a cut along $x_2 = 0$ (right). Due to the rotational symmetry, the cut in every direction looks similar. A simple count of nodal planes along the axes $x_1 = 0$ or $x_2 = 0$ leads to wrong results and does not enable an automated determination of the quantum number.

Table 1
Deviation to the first, fifth and tenth eigenvalue of the 4d harmonic oscillator as a function of the grid-spacing h and the resulting practical order n of the five-point Numerov algorithm.

Number of gridpoints	11	15	19	23	27	31	35	Resulting order n $\mathcal{O}(h^n)$
Gridspacing h	0.1	0.0714	0.0556	0.0455	0.0385	0.0333	0.0294	–
Deviation to EV_1	0.04686	0.02661	0.01172	0.00563	0.00290	0.00199	0.00097	3.2
Deviation to EV_5	0.06963	0.03007	0.01735	0.00909	0.00490	0.00338	0.00171	3.0
Deviation to EV_{10}	0.35203	0.25275	0.11499	0.05693	0.03063	0.01848	0.01094	3.0

Table 2
Vibrational Frequencies of the CO_2 molecule given in cm^{-1} obtained from a 4d-Numerov treatment at different levels of theory compared to harmonic and VPT2 data.

	NM1	NM2	NM3	NM4	MAD
		Harmonic			
B3LYP/6-311 + + G(3df,3pd)	679	679	1374	2414	44
MP2/6-311 + + G(3df,3pd)	673	673	1337	2429	35.5
MP2/cc-pVTZ	656	656	1332	2426	37
CCSD(T)/cc-pVTZ	700	700	1360	2412	35.5
		VPT2			
B3LYP/6-311 + + G(3df,3pd)	674	674	1390	2368	34
MP2/6-311 + + G(3df,3pd)	665	665	1313	2376	15.25
MP2/cc-pVTZ	652	652	1309	2375	19.75
CCSD(T)/cc-pVTZ	–	–	–	–	–
		Numerov			
B3LYP/6-311 + + G(3df,3pd)	679	679	1307	2363	14.5
MP2/6-311 + + G(3df,3pd)	673	673	1286	2385	11.75
MP2/cc-pVTZ	658	658	1269	2383	17.5
CCSD(T)/cc-pVTZ	662	662	1278	2346	7.33
exp[a]	668	668	1285	2349	-
VCI/vibr. force field[b]	667	667	1284	2346	1.5

NM1 and NM2 are describing the bending modes, NM3 the symmetric stretch mode and NM4 the asymmetric stretch mode.
[a] [67].
[b] [68,69].

the experimental values. Comparing the mean absolute deviation (MAD) of the different theory levels the CCSD(T)/cc-pVTZ calculation leads to the results with the smallest deviation as expected. The wavenumbers obtained from the Numerov method show a significant improvement over the harmonic case, reducing the MAD value by a factor of 5 in the CCSD(T) case.

Comparing the results of the VPT2 approach with those obtained via the Numerov treatment highlights an improved description of the fundamental wavenumbers, especially in the B3LYP case (due to the lack of analytical second derivatives, a VPT2 calculation at CCSD(T) level was not possible). Recently, it was discussed that the VPT2 approach is less suitable for strongly anharmonic potentials [7,8]. The data also indicate that the results obtained at the MP2 level are not particularly reliable: while in case of VPT2 the MP2 method performs much better than B3LYP, an opposite trend can be seen in the harmonic and 4d-Numerov case. Also, the MP2/6-311 + + G(3df,3pd) level appears to be more reliable than the MP2/cc-pVTZ level. This results should be considered with caution, however, as they are most likely the consequence of an error compensation in the MP2/6-311 + + G(3df,3pd) case. Overall it can be stated that the B3LYP- and MP2-level lead to similar results, whereas the slightly higher MAD in the MP2 case could be caused by the tendency to overestimate electron correlation effects.

The high MAD value of the MP2 calculations (both basis sets) is mainly caused by the large deviation observed for the wavenumber of the asymmetric stretch mode. Where B3LYP leads to deviations between 11 and 22 cm^{-1}, the range of the MP2 calculation with the same basis set is between 1 and 36 cm^{-1}. The deviations of the MP2 calculation with the correlated basis set is between 10 and 34 cm^{-1}, while the deviations of the CCSD(T) calculation using the correlation-consistent basis are between 3 and 7 cm^{-1} being in the same range as those obtained from a VCI treatment using a vibrational force field, that has been explicitly fitted to reproduce the experimental data [68,69].

For all levels of theory and basis sets the Numerov analysis was applied in one, two and three dimensions and all possible combinations of the respective vibrational modes. Here only the results of the CCSD(T) calculation will be discussed (see Table 3), the other levels of theory show similar results and can be found in the Supplementary Material Tables (S1) to (S3).

In the one-dimensional case only the anharmonicity of the potential energy is considered. Generally, the accuracy of results is increased with every additional dimension taken into account, resulting from the improved consideration of inter-mode coupling in higher dimensions. It

Table 3
Vibrational Frequencies of the CO_2 molecule in different dimensions. All calculations were executed on CCSD(T)/cc-pVTZ level. In the four-dimensional case a 5-point stencil was applied, in all other dimensions a 9-point stencil.

	Vibr. frequencies in 1/cm				Difference to the 4d-Numerov			
	NM1	NM2	NM3	NM4	NM1	NM2	NM3	NM4
harmonic	700	700	1360	2412	38	38	82	67
1D	670	670	1340	2411	8	8	62	66
2D	672	672	–	–	10	10	–	–
	662	–	1296	–	0	–	18	–
	656	–	–	2397	–6	–	–	52
	–	662	1296	–	–	0	18	–
	–	656	–	2397	–	–6	–	52
	–	–	1331	2358	–	–	53	13
3D	663	663	1282	–	1	1	4	–
	659	659	–	2384	–3	–3	–	39
	–	656	1285	2352	–	–6	7	7
	656	–	1285	2352	–6	–	7	7
4D	662	662	1278	2345	–	–	–	–
exp[a]	668	668	1285	2349	6	6	7	4

[a] [67].

can be seen that anharmonicity and mode coupling result in a reduction of the wavenumbers compared to the harmonic treatment. In this case anharmonicity and inter-mode coupling support each other, with both leading to lower wavenumbers in line with the common expectation.

For the asymmetric stretch vibration (NM4) the results of the harmonic and the 1d-Numerov analysis differ only by 1 wavenumber. This is due to the nearly harmonic shape of the potential energy surface in the region near the minimum, implying that the fundamental vibration of NM4 is only influenced by mode-coupling. In the three-dimensional Numerov treatment the same trend can be observed: The symmetric stretch mode (NM3) has a high deviation to the four-dimensional result of 62 cm^{-1}(4.8%) in one dimension and 53 cm^{-1} (4.14%) in two dimensions. This deviation is significantly smaller in the three-dimensional Numerov analysis (7 cm^{-1} or ≈ 0.5%). For the asymmetric stretch mode (NM4) the deviation to the four-dimensional result is reduced with each added dimension but is still above 1% (39cm^{-1} or 1.6%) in the three-dimensional case if NM3 is not considered. It can be seen that NM4 strongly couples with NM3, while NM3 does not couple with NM4 but only with NM1 and NM2. If NM3 and NM4 are considered in the 3d-Numerov analysis the deviation to the four-dimensional result is below 10 wavenumbers for all frequencies.

This analysis shows, that in lower dimensions also good results are obtained for particular mode combinations. The key problem in this case is that due to the high number of possible combinations of vibrational modes to be investigated it is not possible to decide which results are the ones representing the best prediction. It can also be seen that it is not possible to estimate the four-dimensional result using the sum of the deviations between lower dimensions or by calculating the mean value of the different results in a lower dimension.

Investigating the eigenvectors it is possible to assign the vibrational frequencies to their respective excited states, or their quantum number, respectively. Most of the states can be assigned without problems analogous to the one-dimensional case where the number of nodes of the eigenfunction is equivalent to the excitation level of the respective state. In the four-dimensional case the assignment had to be done visually. Since it is known that the asymmetric stretch mode (NM4) is at ≈ 2400cm^{-1} all frequencies below this value have to belong to excitations of the bending and symmetric stretch modes. To verify this the wavefunctions were projected to three dimensions and displayed using isosurfaces (corresponding to the wavefunction in the hyperplane $x_4 = 0$). An example for an excited vibrational state can be seen in Fig. 3(a), in which the excitation can be assigned directly to the (1 0 0 0) state. The states (1 1 0 0) and (0 0 1 0) shown in Figs. 3(b) and (c) are examples of two challenging cases in the mode assignment, since they show a radial symmetric wavefunction analogous to the (1 1) state of an ideal two-dimensional harmonic oscillator depicted in Fig. 2. This is a strong argument that the resulting wavefunction for the state (1 1 0 0) is reasonable. Both states can be distinguished by looking for higher excited states (0 0 2 0) and (2 2 0 0) shown in Figs. 3(d), and (e) in which case the wavefunctions have a different shape that can be easily distinguished. Looking at the eigenfunction of the (0 0 2 0) state, the second nodal surface between the positive and negative isosurfaces can be seen. Both states (2 2 0 0) and (0 0 2 0) can be separated from the remaining set, due to the similarities in the bending modes NM1 and NM2 the wavefunctions of the respective overtones are degenerate and the respective eigenvalues appearing two times.

Some of the assigned frequencies can also be observed in the IR-spectrum, but most of the peaks are too small to be clearly identified or separated from the background noise, respectively. All depictions of the projected eigenfunctions with $x_4 = 0$ of the first 15 states shown in Table 4 can be found in the Supplementary Material, Figs. (S1) to (S15).

3.3. BeH_2 – Beryllium hydride

Beryllium hydride was chosen as second target system with four normal modes since it is in addition to CO_2 and HCN one of the most common examples for the vibrational treatment of linear molecules [70]. While both molecules share the same symmetry group ($D_{\infty h}$), the difference to CO_2 is the ratio of atomic masses of the atoms. The BeH_2 molecule was calculated at CCSD(T)/cc-pVQZ level only. A VCI study of Koput and Peterson has shown that the wavenumbers of BeH_2 fundamental are already converged at this level of theory compared to more demanding investigations using cc-pV5Z and cc-pV6Z basis sets [71].

The wavenumbers obtained from the different Numerov levels are shown in Table 5 along with a comparison to experimental IR data and previous theoretical results. The wavenumbers predicted by the four-dimensional Numerov analysis for both bending modes (NM1 and NM2) and the asymmetric stretch mode (NM4) show deviations ⩽ 4 cm^{-1} in all cases. For the Raman active vibrational frequency of the symmetric stretch mode (NM3) no experimental results were availabe

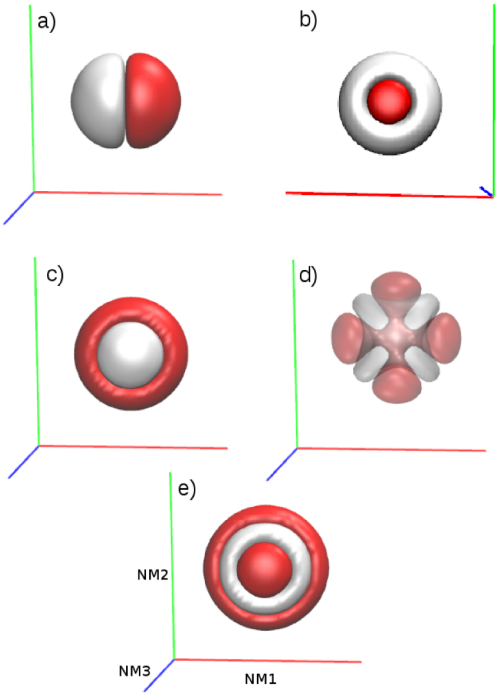

Fig. 3. Isovalue representation of selected four-dimensional vibrational wavefunctions for the CO_2 molecule (CCSD(T) level) projected onto the hyperplane $x_4 = 0$: (a) state 1000; (b) state 1100; (c) state 0010; (d) state 2200; (e) state 0020; The isosurfaces are drawn at ± 0.001. The red axis corresponds to NM1, the green one to NM2 and the blue one to NM3.

Table 4
Assignment of the wavenumbers to the respective excited states of the CO_2 molecule with n_1 to n_4 corresponding to the quantum number of the respective normal mode. The calculation was executed at CCSD(T)/cc-pVTZ level.

#	n_1	n_2	n_3	n_4	wavenumber in 1/cm
0	0	0	0	0	0
1	1	0	0	0	662
2	0	1	0	0	662
3	0	0	1	0	1278
4	0	2	0	0	1324
5	2	0	0	0	1328
6	1	1	0	0	1386
7	1	0	1	0	1923
8	0	1	1	0	1923
9	3	0	0	0	1992
10	0	3	0	0	1992
11	2	1	0	0	2075
12	1	2	0	0	2075
13	0	0	0	1	2346
14	0	0	2	0	2538

Table 5
Vibrational frequencies of the BeH_2 molecule given in cm^{-1}. In the four-dimensional case a 5-point stencil was applied, in all other dimensions a 9-point stencil. The calculation was executed at CCSD(T)/cc-pVQZ level.

	NM1	NM2	NM3	NM4
harm	715	715	2043	2250
1D	740	740	2014	2296
2D	748	748	–	–
	713	–	2014	–
	709	–	–	2261
	–	713	2014	–
	–	709	–	2261
	–	–	1986	2191
3D	716	716	2014	–
	718	718	–	2228
	–	699	1986	2177
	699	–	1986	2177
4D	702	702	1986	2162
exp.	698[a]	698[a]	–	2159[a]/2178[b]
CCSD(T)/ANO/ VPT2[c]	716	716	1980	2167
CCSD(T)/cc-pVTZ/ VCI[d]	705	705	1987	2158
CCSD(T)/cc-pV6Z/ VCI[e]	713	713	1985	2171

[a] [70].
[b] [75].
[c] [72].
[d] [73].
[e] [71].

in the literature. Comparison to VPT2 and VCI data based on CCSD(T) calculations [72,73,71] shows a deviation from 1 to 7 cm^{-1}, while the other three normal modes (NM1, 2 and 4) deviate in the range of 3–14 cm^{-1}. However, since in the case of these vibrations the Numerov approach leads to a similar or even better agreement with experimental results, the same can be assumed for NM3.

In addition to the four-dimensional analysis, Numerov's method was also applied to lower dimensions. The one-dimensional results show in all modes except the symmetric stretch mode (NM3) higher deviations to the four-dimensional Numerov analysis than the harmonic approach. In the two-dimensional case the results for both stretch modes are lowered. The result for the bending modes is higher than in the one-dimensional case except when they are combined with one of the stretching modes. If combined with the asymmetric stretching mode (NM4) both frequencies are lowered by ≈ 30cm^{-1}. The bending modes combined with the symmetric stretch mode (NM3) yields a smaller wavenumber for the bending mode (− 27 cm^{-1}) while the result for NM3 is the same as the in one dimensional case. This suggests a strong coupling between the different modes, which is visible already in the three-dimensional case. The data of the calculations lead to a good agreement with experimental results, if both stretching modes are considered. The deviation to experimental data is increased only if one stretching mode is included.

The results show, that the Numerov analysis yields small deviations to the experimental data. In lower dimensions there exist combinations which lead to nearly similar results, but again the problem is that due to the many possible combinations it is not obvious which is the most suitable one to predict a certain frequency using only the two- or three-dimensional results.

A further highly interesting observation is the fact that for NMs 1, 2 and 4 the anharmonicity shifts the frequency to higher wavenumbers. This situation is counterintuitive to the common perception that anharmonicity always leads to lower wavenumbers. The reason for the observed increase is linked to a higher order potential energy surface (*i.e.* quartic, sextic, etc), which is a different kind of anharmonicity compared to a Morse-anharmonic potential leading to a decrease of the difference between the subsequent eigenstates. Application of a higher dimensional Numerov treatment leads to a frequency shift in the opposite direction, thus in case of NMs 1, 2 and 4 anharmonicity and inter-mode coupling counteract each other. Similar findings are also discussed in [74] studying the vibrational spectra of gold and silver clusters via VSCF.

Table 6
Mode assignment for the BeH_2 molecule with n_1 to n_4 corresponding to the quantum number of the respective normal mode. The calculation was executed at CCSD(T)/cc-pVQZ level.

#	n_1	n_2	n_3	n_4	wavenumber in 1/cm
0	0	0	0	0	
1	1	0	0	0	702
2	0	1	0	0	702
3	1	1	0	0	1398
4	0	2	0	0	1408
5	2	0	0	0	1408
6	0	0	1	0	1986
7	2	1	0	0	2098
8	1	2	0	0	2098
9	3	0	0	0	2119
10	0	3	0	0	2119
11	0	0	0	1	2162
12	1	0	1	0	2688
13	0	1	1	0	2688
14	2	2	0	0	2794

Analogous to the CO_2 case the frequencies were assigned to the different excited states (see Table 6). All wavefunctions show a similar shape than the ones observed for carbon dioxide. Because of the different mass ratio between the atoms the order of the states (0 0 1 0) and (1 1 0 0) is interchanged. The (1 1 0 0) state is now the one with the lower frequency and therefore, also the higher excitations containing one of both ground states appear in different order.

3.4. HCN

As in the other two target systems the results of the Numerov analysis in various dimensions are compared to the harmonic approximation and to experimental data. The potential energy grid was created at CCSD(T)/cc-pVTZ level and evaluated in one to four dimensions using the Numerov treatment. In Table 7 the harmonic frequencies, the respective Numerov results and corresponding experimental data are shown. One can see that the harmonic frequencies for the bending modes (NM1 and 2) have a very small deviation to experimental data (4 cm^{-1}), while the one-dimensional Numerov analysis shows a deviation of more than 100 wavenumbers. The higher deviation of the Numerov analysis in one and (partly) in two dimensions is the influence of the considered anharmonicity. Analogous to NMs 1, 2 and 4 in the BeH_2

Table 7
Vibrational wavenumbers of the HCN molecule in cm^{-1}. In the four-dimensional case a 5-point stencil was applied, while in all other dimensions a 9-point stencil was used. The potential energy was calculated at CCSD(T)/cc-pVTZ level.

	NM1	NM2	NM3	NM4
harm	716	716	2111	3444
1D	832	832	2092	3366
2D	859	859	–	–
	830	–	2094	–
	714	–	–	3357
	–	830	2094	–
	–	714	–	3357
	–	–	2085	3339
3D	856	856	2097	–
	724	724	–	3352
	–	710	2083	3336
	710	–	2083	3336
4D	719	719	2082	3331
exp.[a]	712	712	2089	3312

[a] [76].

case in this example the frequencies shift to higher wavenumbers, again caused by higher-order anharmonicity. Since the harmonic approximation neglects anharmonicity as well as inter-mode coupling, the good agreement of the harmonic approximation data with experimental results is due to a fortnitous coincidence resulting in a near-perfect cancellation of anharmonicity and mode-mode coupling effects.

If the bending modes are combined with the C–H stretching mode (NM4) the inter-mode coupling shifts the frequency back to the region of the four-dimensional Numerov analysis. This example shows the strong influence of anharmonicity and inter-mode coupling shifting the respective frequency again in opposite directions similar as observed for BeH_2. The C–H stretching vibration shows a different behavior: the deviation to the experimental results is decreasing for increasing dimensions. For the C-N stretching vibration the difference between the two- and three-dimensional results is very small ($2cm^{-1}$ each). The influence of the considered anharmonicity (1d and higher) and inter-mode coupling (2d and higher) is much smaller for both stretching modes, but can still be observed. For the four-dimensional Numerov analysis all fundamental bands show a deviation of less than 1% to the experimental data with the largest difference being $20cm^{-1}$ for NM4. This is due to the complex electronic structure of the C-N triple bond. Despite the correlated CCSD(T) treatment the low reduced mass of NM4 of 1.18 g/mol makes this normal mode highly sensitive to inaccuracies in the potential energy surface. Also the lower dimensional calculations for particular mode combinations show deviations below 1% (except the 1d analysis). Due to the many possible combinations in lower dimensions it can again not be decided which results are the most suitable ones. At present there is no possibility to provide an estimation of the frequency (of the four-dimensional analysis) using only the lower dimensional results.

Similar as in the previous examples the frequencies of the HCN molecule have been assigned based to the respective excitation level listed in Table 8. Most of the wavefunctions show a similar shape as observed in case of CO_2 and BeH_2. The main difference is that the states (0 0 1 0) and (1 1 0 0) can be easily distinguished without considering excited states of higher order.

In [76] the rotational-vibrational spectra of HCN was measured. The resulting vibrational frequencies are given also for the overtones of the bending modes (1412 cm^{-1} and 2117 cm^{-1}). The results of the four-dimensional analysis show deviations of $\approx 40\ cm^{-1}$ for the first and $\approx 100\ cm^{-1}$ for the second overtone. This deviations are higher than for the fundamental ones and could be result of the neglected rotation-vibration coupling in the Numerov approach. Nevertheless, these results demonstrate that the Numerov analysis is also suitable to characterize frequencies of higher excited states.

Table 8
Mode assignment of the HCN molecule. The respective potential energy surface was constructed at CCSD(T)/cc-pVTZ level.

#	1	2	3	4	wavenumber in 1/cm
0	0	0	0	0	
1	1	0	0	0	719
2	0	1	0	0	719
3	1	1	0	0	1452
4	0	2	0	0	1456
5	2	0	0	0	1457
6	0	0	1	0	2083
7	3	0	0	0	2215
8	0	3	0	0	2215
9	2	1	0	0	2217
10	1	2	0	0	2217
11	1	0	1	0	2802
12	0	1	1	0	2802
13	4	0	0	0	2998
14	0	4	0	0	2998
15	3	1	0	0	3008
16	1	3	0	0	3011
17	2	2	0	0	3013
18	0	0	0	1	3331

3.5. Interpolation

This article focuses on the presentation of the adapted Numerov approach in four dimensions and its performance. Nevertheless, the time-consuming calculation of the gridpoints may prove as a limiting factor. To overcome this problem interpolation can be applied. Especially in higher dimensions the number of gridpoints to be calculated is drastically reduced by incresing the stepsize by the factor of two to three by interpolation. This largely reduces the number of quantum chemical potential evaluations by up to 98% in the presented examples. For each test system the gridspacing h was increased by the factor of two and three based on the calculated grids and interpolated in the following applying cubic splines by applying the “interpn” function of the program MATLAB [77]. The wavenumbers for CO_2, BeH_2 and HCN obtained from the different interpolation settings are given in Table 9. One can see that, depending on the PES, the interpolation only slightly changes the resulting wavenumbers. The number of gridpoints to be calculated is reduced by 93%(double gridspacing) and ≈ 98.4% (triple gridspacing), respectively. The results show, that spline interpolation is an alternative when the computational demand has to be reduced. Nevertheless, every application of interpolation may pose as a potential error source that can lead to less accurate results. Therefore, a compromise in between computational demand and accuracy has to be found. Especially the increase of the stepsize by a factor of two proved as a reliable strategy, reducing the number of QM calculations by more than 90% while the obtained wave numbers are virtually identical to those obtained using the fully calculated PES, in particular in case of BeH_2 and HCN.

4. Conclusion

In this work the extension of the adapted Numerov approach [42] to four dimensions was derived and implemented. To the best of our knowledge it is the first time a four-dimensional Numerov approach to solve the Schroedinger equation was presented. The resulting wavefunctions were used to assign the vibrational frequencies to their respective excited state or quantum number, respectively. Carbon dioxide, beryllium hydride and hydrogen cyanide, all three common examples for triatomic linear molecules, were investigated employing a hierarchical application of the Numerov approach from a one- to a four-dimensional treatment. This stepwise extension of the methodology enables a detailed analysis of the influence of anharmonicity and the increasing impact of inter-mode coupling.

In addition to the occurrence of higher order anharmonicity shifting the respective wavenumbers to higher values, the detailed analysis of

Table 9
Wavenumbers (in 1/cm) for the three test systems obtained by interpolation by increasing the gridspacing h by the factor of two and three, respectively.

Grid to be calculated	Total gridpoints	NM1	NM2	NM3	NM4
	CO_2				
49 × 49 × 25 × 25	1500625	662	662	1278	2346
25 × 25 × 13 × 13	105625(7%)	659	659	1272	2336
17 × 17 × 9 × 9	23409(1.6%)	659	659	1272	2335
	BeH_2				
49 × 49 × 19 × 17	775523	702	702	1986	2162
25 × 25 × 10 × 9	56250(7%)	702	702	1988	2162
17 × 17 × 7 × 6	12138(1.6%)	702	702	1989	2176
	HCN				
45 × 45 × 47 × 15	1427625	719	719	2083	3331
23 × 23 × 24 × 8	101568(7%)	719	719	2083	3331
15 × 15 × 16 × 5	18000(1.2%)	722	722	2086	3348

mode-mode coupling via 2d-, 3d- and 4d-Numerov implementation demonstrates that inter-mode coupling does not always follow a one-to-one correspondence. It is indeed possible that a particular mode is strongly influenced, while the impact on the other mode is of much smaller magnitude, highlighting an entire new facet of vibrational coupling.

For all three target systems the four-dimensional Numerov analysis at CCSD(T)/cc-pVnZ (n = Q, T) level achieved deviations of less than 1% compared to experimental data. In case of CO_2 the four different theoretical levels applied to construct the potential energy surface led to MAD-values with respect to experiment being much smaller than those obtained for the corresponding VPT2 calculations.

The lower dimensional Numerov analyses (*i.e.* 2d and 3d) showed that for particular combinations of normal modes reliable results with only small deviations to the four-dimensional result can be achieved. However, due to the large number of possible combinations it is not feasible to predict which agrees best with experimental data, *i.e.* without further information about the population of the vibrational states it is not possible to estimate the 4d-wavenumbers using only the two- or three-dimensional results.

A further strategy to greatly reduce the computational demand is interpolation of the PES, being applied also in other approaches for the calculation of vibrational frequencies [18,78]. In most cases interpolation leads to results of similar accuracy range as the fully computed PES while reducing the computational demand by up to 98 %. Nevertheless the accuracy decreases due to the additional approximation inherent to the interpolation of the gridpoints. In this paper the main focus lies on the performance of the adapted Numerov approach and the results of the interpolation are only mentioned to point out the possibility of reducing the computational demand.

It is envisaged that the accuracy of the four-dimensional approach is improved in future application by applying larger stencils. In this work the size of the matrix problem already proved to be highly challenging for the eigensolver routine. Although the single point calculations to create the potential energy grid are perfectly parallisable the demand of the computational demand grows exponentially with additional dimensions. The next step should therefore focus on an approach to estimate the population using lower dimensional frequency analysis, as suggested in [79,80] for two dimensions. Using this information it could be possible to approximate higher-dimensional calculations with the results of the lower dimensional analysis, which would lead to a dramatic reduction of the computational demand, with the presented 4d-Numerov results acting as the respective reference data.

A particular benefit of grid-based approaches is the possibility to apply the approach in studies of individual modes. A typical example are applications in the regime of near-infrared spectroscopy (NIR). The latter method is sometimes referred to as “XH-spectroscopy” [81] since the main bands observable in the NIR-range are overtones and combination bands resulting from hydroxy and amine/imine functional groups of organic molecules. The theoretical treament of NIR modes is comparably challenging due to the dominant impact of anharmonicity effects and intermode coupling, rendering an approach based on the harmonic approximation in many cases inadequate. Since on the other hand, only a subset of vibrational modes is relevant to evaluate the properties of NIR-bands, an approach focusing on these vibrational modes appears highly promising. For instance, in case of molecules carrying a single OH group, a 1d-Numerov treatment proved adequate to achieve very good agreement in the calculated wave number not only for the fundamental but also for the first overtone wave number [55]. Higher order Numerov frameworks enable both an extension of the method to consider several, coupled functional groups at the same time (e.g. in case of polyalcohols/polyphenols) or/and improve upon the existing capabilities by considering also relevant vibrations that may couple with the mode of interest. Typical examples in the latter case are the C-O stretch as well as the C–O–H bending vibrations that may show intermode coupling with the O–H stretch in an alcohol/phenol molecule.

A second highly relevant area of research that may benefit substantially from the presented 4d-Numerov implementation lies in the regime of solid-state chemistry [82]. Surface structures of metals and metal oxides in contact with liquids or other compounds such as H_2(g) may show the formation of surface hydroxy groups (e.g. via corrosion). Due to its non-invasive properties infrared spectroscopy provides a suitable route to study the composition and concentration of OH groups located at the surface, for instance in experiments requiring a controlled pressure environment. The theoretical treatment of such systems benefits strongly from including a large number of atoms in the solid-state part to achieve a good approximation of the surface structure in contact with the bulk of the solid. This on the other hand increases the total number of degrees of freedom and the associated number of vibrational modes. The possiblity to focus exclusively on the properties of the surface groups in the theoretical treatment of these systems is of particular advantage, since the vibrational properties of the solid are typically not of particular interest. Higher order Numerov implementations enable for instance the simulataneous treament of two OH groups, considering not only the two OH-stretch degrees of freedom but also the associated OH bending modes with respect to the surface. This can be expected to results in an improved description of complex surface patterns as for instance alternating H-bond structures observed at the surface of SiO_2 [82]. However, since the Numerov method is not limited to applications in spectroscopy, other research questions such as the tunneling properties of H-atoms along a particular reaction coordinate can also benefit strongly from higher order Numerov schemes. Here, the key feature of this method that the functional form of the wave function is not predetermined nor dependent on the choice of a specific set of basis functions represents a further advantage. The detailled benchmarking of the newly developed 4d-Numerov treatment carried out in this study thus provides a key initial step to verify the suitability of the method in the prediction of quantum mechanical properties of molecular compounds.

Acknowledgement

The research was financially supported by the Tyrolean Science Fund (TWF) of the Land Tirol and by *Verein zur Förderung der wissenschaftlichen Ausbildung und Tätigkeit von Südtirolern an der Landesuniversität Innsbruck*. This work was supported by the Austrian Ministry of Science BMWFW as part of the Konjunkturpaket II of the Focal Point Scientific Computing at the University of Innsbruck.

Appendix A. Supplementary data

Supplementary data associated with this article can be found, in the online version, at https://doi.org/10.1016/j.chemphys.2019.01.007.

References

[1] E. Bright Wilson Jr., J.C. Decius, P.C. Cross, Molecular Vibrations – The Theory of Infrared and Raman Vibrational Spectra, Dover Books on Chemistry, 1955.
[2] J.P. Merrick, D. Moran, L. Radom, An evaluation of harmonic vibrational frequency scale factors, J. Phys. Chem. A 111 (45) (2007) 11683–11700.
[3] T. Helgaker, P. Jørgensen, J. Olsen, Molecular Electronic Structure Theory, Wiley, Chichester, 2000.
[4] A. Willetts, N.C. Handy, W.H. Green Jr., D. Jayatilaka, Anharmonic corrections to vibrational transition intensities, J. Phys. Chem. 94 (14) (1990) 5608–5616.
[5] J. Vasquez, J.F. Stanton, Simple algebraic equation for transition moments of fundamental transitions in vibrational second-order perturbation theory, Mol. Phys. 104 (2006) 377–388.
[6] V. Barone, Anharmonic vibrational properties by a fully automated second-order perturbative approach, J. Chem. Phys. 122 (2005) 014108 .
[7] J. Grabska, M.A. Czarnecki, K.B. Bec, Y. Ozaki, Spectroscopic and quantum mechanical calculation study of the effect of isotopic substitution on nir spectra of methanol, J. Phys. Chem. A 121 (2017) 7925–7936.
[8] K.B. Beć, J. Grabska, M.A. Czarneckib, Spectra-structure correlations in nir region: spectroscopic and anharmonic dft study of n-hexanol, cyclohexanol and phenol, Spectrochimica Acta Part A: Mol. Biomol. Spectroscopy 197 (2018) 176–784.

[9] J. Bowman, Self-consistent-field energies and wavefunctions for coupled oscillators, J. Chem. Phys. 68 (1978) 608.
[10] J. Bowman, The self-consistent-field approach to polyatomic vibrations, Acc. Chem. Res. 19 (7) (1986) 202–209.
[11] T.K. Roy, R.B. Gerber, Vibrational self-consistent field calculations for spectroscopy of biological molecules: new algorithmic developments and applications, Phys. Chem. Chem. Phys. 15 (2013) 9468.
[12] O. Christiansen, Vibrational stucture theory: new vibrational wave function methods for calculation of anharmonic vibrational energies and vibrational contributions to molecular properties, PCCP 9 (2007) 2942–2953.
[13] O. Christiansen, Møller-plesset perturbation theory for vibrational wave functions, J. Chem. Phys. 119 (2003) 5773.
[14] N. Matsunaga, G.M. Chaban, R.B. Gerber, Degenerate perturbation theory corrections for the vibrational self-consistent field approximation: Method and applications, J. Chem. Phys. 117 (2002) 3541.
[15] J.O. Jung, R.B. Gerber, Vibrational wave functions and spectroscopy of (h_2o)_n, n=2,3,4,5: Vibrational self-consistent field with correlation corrections, J. Chem. Phys. 105 (1996) 10332.
[16] S. Carter, S.J. Culik, J.M. Bowman, Vibrational self-consistent field method for many-mode systems: a new approach and application to the vibrations of co adsorbed on cu(100), J. Chem. Phys. 107 (1997) 10458.
[17] G. Rauhut, Efficient calculation of potential energy surfaces for the generation of vibrational wave functions, J. Chem. Phys. 121 (2004) 9313.
[18] T. Hrenar, H.-J. werner, G. Rauhut, Accurate calculation of anharmonic vibrational frequencies of medium sized molecules using local coupled cluster methods, J. Chem. Phys. 126 (2007) 134108 .
[19] D.M. Benoit, Fast vibrational self-consistent field calculations through a reduced mode-mode coupling scheme, J. Chem. Phys. 120 (2004) 562.
[20] Y. Scribano, D.M. Benoit, Calculation of vibrational frequencies through a variational reduced-coupling approach, J. Chem. Phys. 127 (2007) 164118 .
[21] N. Gohaud, D. Begue, C. Darrigan, C. Pouchan, New parallel software(p_anhar) for anharmonic vibrational calculations: application to (ch_3li)_2, J. Comput. Chem. 26 (2005) 743–754.
[22] D. Begue, N. Gohaud, C. Pouchan, P. Cassam-Chenai, J. Lievin, A comparison of two methods for selecting vibrational configuration interaction spaces on a heptatomic system: ethylene oxide, J. Chem. Phys. 127 (2007) 164115 .
[23] J.C. Mason, D.C. Handscomb, Chebyshev Polynomials, CRC Press, 2010.
[24] B. Fornberg, A Practical Guide to Pseudospectral Methods, Cambridge University Press, 1998.
[25] D.T. Colbert, W.H. Miller, A novel discrete variable representation for quantum mechanical reactive scattering via the s-matrix kohn method, J. Chem. Phys. 96 (3) (1992) 1982–1991.
[26] A. Bulgac, M. McNeil Forbes, Use of the discrete variable representation basis in nuclear physics, Phys. Rev. C 87 (2013).
[27] L. Laaksonen, P. Pyykkö, D. Sundholm, Fully numerical Hartree-Fock methods for molecules, Computer Phys. Rep. 4 (1986) 313–344.
[28] P. Pyykkö, Fully numerical solution of Hartree-Fock and similar equations for diatomic molecules, in: A.J. Kallio, E. Pajanne, R.F. Bishop (Eds.), Recent Progress in Many-Body Theories, vol. 1, Plenum Press, New York, 1988, pp. 349–355.
[29] P. Pyykkö, Fully numerical calculations for diatomic systems, in: M. Defranceschi, J. Delhalle (Eds.), Numerical Determination of the Electronic Structure of Atom Diatomic and Polyatomic Molecules, Kluwer, Dordrecht, 1989, pp. 161–175.
[30] P. Pyykkö. Fully numerical Hartree-Fock methods for molecules. In K. Kankaala and R. Nieminen, editors, Scientific Computing in Finland, pages 183–213. CSC Res. Report R1/89, Espoo, 1989.
[31] P. Pyykkö, D. Sundholm, L. Laaksonen, J. Olson, Two fully numerical methods in quantum chemistry, in: A. Tenner (Ed.), The CP 90 Europhysics Conference on Computational Physics, World Scientific, Singapore, 1991, pp. 455–457.
[32] E.A. McCullough Jr., Numerical Hartree-Fock methods for molecules, in: P. von Rague Schleyer (Ed.), Encyclopedia of Computational Chemistry, Wiley, Chichester, 1998, pp. 1941–1947.
[33] L. Frediani, D. Sundholm, Real-space numerical grid-methods in quantum chemistry, Phys. Chem. Chem. Phys. 17 (47) (2015) 31357–31359.
[34] Jeremiah R. Jones, François-Henry Rouet, Keith V. Lawler, Eugene Vecharynski, Khaled Z. Ibrahim, Samuel Williams, Brant Abeln, Chao Yang, William McCurdy, Daniel J. Haxton, Xiaoye S. Li, Thomas N. Rescigno, An efficient basis set representation for calculating electrons in molecules, Mol. Phys. 114 (13) (2016) 2014–2028.
[35] B.V. Numerov, Méthode nouvelle de la determination des orbites et le calcul des éphémé rides en tenant compte des perturbations, Publications de l'Observatoire Astrophysique Central de Russie 2 (1923) 188–288.
[36] B.V. Numerov, A method of extrapolation of perturbations, Monthly Notices R. Astron. Soc. 84 (1924) 592–601.
[37] H. Grubmüller, T. Graen, Nusol – numerical solver for the 3d stationary nuclear schrödinger equation, Comput. Phys. Commun. 198 (2016) 169–178.
[38] M. Eckert, Solving the 1-, 2- and, 3-dimensional schrödinger equation for multiminima potentials using the numerov-cooley method. an extrapolation for energy eigenvalues, J. Comput. Phys. 82 (1989) 147–160.
[39] B.R. Johnson, New numerical methods applied to solving the one-dimensional eigenvalue problem, J. Chem. Phys. 67 (1977) 4086.
[40] C.E. Dykstra, D.J. Malik, Derivative numerov-cooley theory. a method for finding vibrational state properties of diatomic molecules, J. Chem. Phys. 87 (1987) 2807.
[41] B. Fornberg, Generation of finite difference formulas on arbitrarily spaced grids, Math. Comput. 51 (184) (1988) 699–706.
[42] U. Kuenzer, J.A. Soraru, T.S. Hofer, Pushing the limit for the grid-based treatment of schrödingers's equation: a sparse numerov approach for one, two and three dimensional quantum problems, PCCP 18 (46) (2016) 31521–31533.
[43] J.C. Light, I.P. Hamilton, J.V. Lill, Generalized discrete variable approximation in quantum dynamics, J. Chem. Phys. 82 (1985) 1400.
[44] J.V. Lill, G.A. Parker, J.C. Light, The discrete variable-finite basis approach to quantum scattering, J. Chem. Phys. 85 (1986) 900.
[45] R. Dawes, T. Carrington Jr., A multidimensional discrete variable representation basis obtained by simultaneous diagonalization, J. Chem. Phys. 121 (2004) 726.
[46] J.C. Light, T. Carrington Jr., Discrete-variable representation and their utilization, Adv. Chem. Phys. 114 (2007) 263–310.
[47] R.G. Littlejohn, M. Cargo, T. Carrington, K.A. Mitchell, B. Poirier, A general framework for discrete variable respresentation basis sets, J. Chem. Phys. 116 (2002) 8691.
[48] V. Szalay, Discrete variable representation of differential operators, J. Chem. Phys. 99 (1993) 1978.
[49] M.J. Bramley, T. Carrington, A general discrete variable method to calculate vibrational energy levels of three- and four-atom molecules, J. Chem. Phys. 99 (1993) 8519.
[50] D. Luckhaus, 6d vibrational quantum dynamics: generalized coordinate discrete variable representation and (a)diabatic contraction, J. Chem. Phys. 113 (2000) 1329.
[51] M. Mladenović, Discrete variable approaches to tetratomic molecules part i: Dvr(6) and dvr(3)+dgb methods, Spectrochimica Acta Part A 58 (2002) 795–807.
[52] D. Lemoine, The finite basis representation as the primary space in multidimensional pseudospectral schemes, J. Chem. Phys. 101 (1994) 10526.
[53] X.-G. Wang, T. Carrington Jr., A finite basis representation lanczos calculation of the bend energy levels of methane, J. Chem. Phys. 118 (2003) 6946.
[54] J.A. Bentley, R.E. Wyatt, A finite basis-discrete variable representation calculation of vibrational levels of planar acetylene, J. Chem. Phys. 97 (1992) 4255.
[55] M.J. Schuler, T.S. Hofer, C.W. Huck, Assessing the predictability of anharmonic vibrational modes at the example of hydroxyl groups - ad hoc construction of localised modes and the influence of structural solute-solvent motifs, PCCP 19 (19) (2017) 11990–12001.
[56] Z. Kalogiratou, Th. Monovasilis, T.E. Simos, Numerical solution of the two-dimensional time independent schrödinger equation with numerov-type methods, J. Math. Chem. 37 (3) (2005) 271–279.
[57] Intel Math Kernel Library for Linux OS - Developer Guide.
[58] R.B. Lehoucq, D.C. Sorensen, C. Yang, ARPACK Users Guide: Solution of Large-Scale Eigenvalue Problems with Implicitly Restarted Arnoldi Methods, SIAM, 1987.
[59] C. Sanderson, R. Curtin, Armadillo: a template-based c++ library for linear algebra, J. Open Source Softw. 1 (2016) 26.
[60] M.J. Frisch, G.W. Trucks, H.B. Schlegel, G.E. Scuseria, M.A. Robb, J.R. Cheeseman, G. Scalmani, V. Barone, B. Mennucci, G.A. Petersson, H. Nakatsuji, M. Caricato, X. Li, H.P. Hratchian, A.F. Izmaylov, J. Bloino, G. Zheng, J.L. Sonnenberg, M. Hada, M. Ehara, K. Toyota, R. Fukuda, J. Hasegawa, M. Ishida, T. Nakajima, Y. Honda, O. Kitao, H. Nakai, T. Vreven, J.A. Montgomery Jr., J.E. Peralta, F. Ogliaro, M. Bearpark, J.J. Heyd, E. Brothers, K.N. Kudin, V.N. Staroverov, R. Kobayashi, J. Normand, K. Raghavachari, A. Rendell, J.C. Burant, S.S. Iyengar, J. Tomasi, M. Cossi, N. Rega, J.M. Millam, M. Klene, J.E. Knox, J.B. Cross, V. Bakken, C. Adamo, J. Jaramillo, R. Gomperts, R.E. Stratmann, O. Yazyev, A.J. Austin, R. Cammi, C. Pomelli, J.W. Ochterski, R.L. Martin, K. Morokuma, V.G. Zakrzewski, G.A. Voth, P. Salvador, J.J. Dannenberg, S. Dapprich, A.D. Daniels, Ö. Farkas, J.B. Foresman, J.V. Ortiz, J. Cioslowski, D.J. Fox, Gaussian-09 Revision D.01, Gaussian Inc., Wallingford CT (2009).
[61] W. Humphrey, A. Dalke, K. Schulten, Vmd – visual molecular dynamics, J. Molec. Graphics 14 (2018) 33–38.
[62] A.D. Becke, Density-functional thermochemistry. III. The role of exact exchange, jcp 98 (1993) 5648–5652.
[63] R. Krishnan, J.S. Binkley, R. Seeger, J.A. Pople, Self-consistent molecular orbital methods. XX. A basis set for correlated wave functions, jcp 72 (1980) 650–654.
[64] C. Møller, M.S. Plesset, Mp/n, Phys. Rev. 46 (1934) 618.
[65] T.H. Dunning Jr, Gaussian basis sets for use in correlated molecular calculations. I. The atoms boron through neon and hydrogen, J. Chem. Phys. 90 (1989) 1007.
[66] R.J. Bartlett, M. Musiał, Coupled-cluster theory in quantum chemistry, Rev. Mod. Phys. 79 (2007) 291.
[67] R.J. Meyer, Kohlenstoff: Teil C - Lieferung 1, Springer, 2013.
[68] E. Mátyus, G. Czakó, B.T. Sutcliffe, A.G. Csaszar, Vibrational energy levels with arbitrary potentials using the eckart-watson hamiltonians and the discrete variable representation, J. Chem. Phys. 127 (2007) 084102 .
[69] A. Chedin, The carbon dioxide molecule – Potential, spectroscopic, and molecular constants from its infrared spectrum, J. Mol. Spectrosc. 76 (1979) 430–491.
[70] T.J. Tague, L. Andrews, J. Am. Chem. Soc. 115 (1993) 12111.
[71] H. Koput, K.A. Peterson, J. Chem. Phys. 125 (2006) 044306 .
[72] J.M.L. Martin, T.J. Lee, Chem. Phys. Lett. 200 (1992) 502.
[73] T. Hrenar, H.-J. Werner, G. Rauhut, PCCP 7 (2005) 3123–3125.
[74] L.A. Mancera, D.M. Benoit, Vibrational anharmonicity of small gold and silver clusters using the vscf method, Phys. Chem. Chem. Phys. 18 (2016) 529.
[75] A. Shayesteh, K. Tereszchuk, P.F. Bernath, J. Chem. Phys. 118 (2003) 3622.
[76] C.R. Keedy, The rotational-vibrational spectra of hcn and dcn: a physical chemistry experiment, J. Chem. Edu. 69 (1992) A296.
[77] MATLAB.R2017b.The MathWorks Inc., Natick, Massachusetts, 2017.

[78] T. Petrenko, G. Rauhut, A new efficient method for the calculation of interior eigenpairs and its application to vibrational structure problems, J. Chem. Phys. 146 (2017) 124101 .
[79] S.K. Gregurick, G.M. Chaban, R.B. Gerber, Ab initio and improved empirical potentials for the calculation of the anharmonic vibrational states and intramolecular mode coupling of n-methylacetamide, J. Phys. Chem. A 106 (37) (2002) 8696–8707.
[80] Y. Miller, G.M. Chaban, R.B. Gerber, Ab initio vibrational calculations for h2so4 and h2so4 h2o: spectroscopy and the nature of the anharmonic couplings, J. Phys. Chem. A 109 (2005) 6565–6574.
[81] Y. Ozaki, Near-infrared spectroscopy – its versatility in analytical chemistry, Anal. Sci. 28 (2012) 545–563.
[82] U. Kuenzer, M. Klotz, T.S. Hofer, Probing vibrational coupling via a grid-based quantum approach-an efficient strategy for accurate calculations of localized normal modes in solid-state systems, J. Comp. Chem. 39 (26) (2018) 2196–2209.